JOURNAL OF GEOPHYSICAL RESEARCH, VOL. 115, C07018, doi:10.1029/2009JC005760, 2010

The role of intratidal oscillations in sediment resuspension in a diurnal, partially mixed estuary

J. M. O'Callaghan,[1,2] C. B. Pattiaratchi,[1] and D. P. Hamilton[3]

Received 27 August 2009; revised 10 March 2010; accepted 7 April 2010; published 29 July 2010.

[1] Using detailed observations of the mean and turbulent properties of flow, salinity and turbidity that spanned 2001/02, we examined the physical mechanisms underpinning sediment resuspension in the low-energy Swan River estuary, Western Australia. In this diurnal tidally-dominated estuary, the presence of intratidal oscillations, a tidal inequality lasting 2 to 3 hours on the flood tide, generated by interactions of the four main diurnal and semidiurnal astronomical constituents, K_1, O_1, M_2, and S_2, played a major role in modifying vertical stratification and mixing. These intratidal oscillations are controlled by phase differences between the tropic and synodic months rather than being temporally-fixed by bed friction, as occurs in semidiurnal estuaries. Intratidal oscillations are largest, at around 0.1 m, near to the Austral solstice when the lunar and solar declination are in-phase. Despite the seemingly small change in water level, shear-induced interfacial mixing caused destratification of the water column with the top-to-bottom salinity (ΔS) difference of 3.5 present early in the flood tide eroded to less than 0.3 by the end of the intratidal oscillation. High turbidity peaks, of 250 nephelometric turbidity units, coincided with these intratidal oscillations and could not be explained by bed friction since shear stress from mean flow did not exceed threshold criteria. High Reynolds stresses of ~1 Nm^{-2} did, however, exceed τ_{cr} and together with negative Reynolds fluxes indicate a net downward transport of material. Destratification of the water column induced by shear instabilities resulted in large overturns capable of moving in situ material towards the bed during intratidal oscillations and these turbidities were ~10 times greater than those from bed-generated resuspension observed later during the flood tide.

Citation: O'Callaghan, J. M., C. B. Pattiaratchi, and D. P. Hamilton (2010), The role of intratidal oscillations in sediment resuspension in a diurnal, partially mixed estuary, *J. Geophys. Res.*, *115*, C07018, doi:10.1029/2009JC005760.

1. Introduction

[2] Estuarine variability is dominated by cyclical tidal oscillations that propagate from the adjacent continental shelf into the estuary [*Uncles*, 2002]. The physical attributes of an estuary, at least in a semidiurnal system, produce tidal asymmetries that strengthen advection, which in turn influences the timing and amplitude of sediment resuspension events [*van de Kreeke et al.*, 1997; *Dyer*, 1997]. In low-energy tidal systems (i.e., microtidal or diurnal) the dominant mechanisms deviate from these paradigms and smaller perturbations in flow and stratification become increasingly important [*Blanton et al.*, 2003; *Becker et al.*, 2009]. Not only are there fewer observations in low-energy estuaries, but the interactions between the mean and turbulent processes are not well observed regardless of tidal range. Thus, greater understanding of both the physical processes and how they regulate material transport is crucial for determining the functioning and impacts of anthropogenic stresses in these threatened systems [*Cooper and Brush*, 1993]. Here, we seek to address this shortcoming using an observational approach to evaluate how mean flows influence turbulence in a low-energy system, while at the same time examining the variability of the less common diurnal tide within estuaries.

[3] Boundary forcing by tidal oscillations or freshwater discharges, or both, govern the longitudinal density gradients in most estuaries. Interactions between advection and mixing further control the temporal variations in salinity. Cyclical tidal action influences not only mean flow, but also the occurrence of vertical mixing. Increased turbulence with spring tides tends to weaken baroclinic flows and vice-versa for neap tides [*Stacey et al.*, 2001]. Vertical shear can increase stratification over the ebb tide, while on the flood tide the reverse can happen and vertical shear can weaken stratification, a phenomenon defined as tidal straining by *Simpson et al.* [1990]. Interplay between mean and turbulent processes can cause transport fluxes of salt or material to

[1]School of Environmental Systems Engineering, University of Western Australia, Crawley, Western Australia, Australia.
[2]Now at National Institute of Water and Atmosphere, Wellington, New Zealand.
[3]Department of Biological Sciences, University of Waikato, Hamilton, New Zealand.

0148-0227/10/2009JC005760

deviate from the tidally-driven mechanisms [*Weisberg and Zheng*, 2003]. For example, *Becker et al.* [2009] observed stronger estuarine circulation on spring tides due to greater near-bottom salinity gradients, while *Nepf and Geyer* [1996] found that active mixing was confined to the near-bed region, rather than over the entire water column. Together, observations of the predictable and anomalous behavior consolidate and improve our knowledge of estuarine dynamics.

[4] Diurnal tides are regulated by the tropic month and result in varying contributions from the diurnal component of the tide. When the moon is at the maximum semimonthly declination (either north or south of the equator), contributions from the diurnal forcing are greatest resulting in tropic tides with high tidal range; when the moon crosses the equator, the diurnal influence is minimal and equatorial tides with low tidal range occur. The period of the tropic month is 27.3 days from perigee to perigee [*Hodgkin and Di Lollo*, 1958; *Pugh*, 1987]. This differs from semidiurnal tides that are controlled by the position of the moon in the sun-earth system with a synodic period (from new moon to new moon) of 29.5 days. Diurnally-dominated tidal systems are restricted to a handful of locations globally and consequently most analyzes of tidal effects have been theoretical [*Ranasinghe and Pattiaratchi*, 2000; *Hoitink et al.*, 2003; *Woodworth et al.*, 2005]. The dominant astronomical constituents in diurnal systems are the O_1 and K_1, which have periods of 25.82 and 23.93 hours, respectively [*Pugh*, 1987]. Propagation of these diurnal tidal waves into shallower water generates harmonics with periods close to 12 hours, which have a similar frequency to the M_2 and S_2 semidiurnal constituents [*Ranasinghe and Pattiaratchi*, 2000]. Contributions by the main semidiurnal constituents mask the contribution by diurnal harmonics, a major point of difference from semi-diurnal systems, with the astronomical tides rather than non-linear interactions between the M_2 and M_4 constituents [*Aubrey and Speer*, 1985] regulating tidal asymmetry in estuaries with diurnal tides. This leads to fluctuations in tidal asymmetry between flood and ebb dominance through an annual cycle, rather than a fixed asymmetry induced by bottom friction as occurs in semidiurnal systems. In diurnal estuaries maximum sediment transport, based on available conventions, were associated with the strongest asymmetry, i.e., the largest tidal currents [*Ranasinghe and Pattiaratchi*, 2000].

[5] Processes governing material transport which operate within low-energy systems are often different and not simply the application of a scaled down version of processes from more energetic systems. Traditionally, sediment entrainment and resuspension occurs when near-bed shear stresses exceed a critical threshold, which in high energy estuaries is coincident with faster currents induced by flood or ebb tidal asymmetries [*Dyer*, 1997]. Since tidal currents in microtidal estuaries are weak, bed shear stresses from mean currents are less likely to exceed critical thresholds for erosion of bed sediments. Other mechanisms such as biological mediation (although not exclusive to low energy estuaries [*Wright et al.*, 1997]) or vertical mixing must be considered to understand the controls on resuspension in low-energy estuaries [*van der Ham et al.*, 2001].

[6] In this paper, we aim to identify the dominant processes which govern sediment resuspension in a low-energy diurnal tidal estuary. In particular, what mechanisms are responsible for eroding bed sediments when mean currents are lower than critical levels to initiate sediment transport? To this end, we first investigated the variability of diurnal tides at the fortnightly and intratidal timescales through an observational campaign that spanned two years. To our knowledge, such a detailed observational study of diurnal tidal variability has not previously been conducted. Although diurnal tidal systems are more unusual, understanding these mechanisms is not only relevant to other low-energy systems, but also important for understanding complexities in high energy systems that would otherwise be masked. Mean and turbulent observations in the upper Swan River estuary in 2001 and 2002 found that the seemingly small, yet regular tidal inequalities, herein called intratidal oscillations, played a major role in vertical mixing, stratification, and ultimately elevated turbidities. The remainder of the paper is constructed as follows. Section 2 presents the intricacies of the field site. Section 3 describes the various instruments used and their set-up. Results for both sampling years are intertwined in Section 4, with a discussion of the governing diurnal tide and mechanisms for sediment transport in a low energy estuary given in Section 5. A summary of the observational findings follow in section 6.

2. Study Site

[7] The Swan River is a partially mixed, microtidal estuary, which bisects the city of Perth, Western Australia, and discharges into the Indian Ocean near Fremantle (top inset, Figure 1). The region has a Mediterranean climate, with hot, dry summers and cool, wet winters. Almost 80% of the annual mean rainfall of 870 mm falls from winter to early spring (May to September), with negligible rainfall in the summer. The estuary catchment area is 121,000 km^2, with most (85%) of the discharge from the Avon River catchment [*Peters and Donohue*, 2001]. Discharge salinity from the Avon River is elevated above that of fresh water, usually 2 to 4 ppt, because of drainage into the catchment from naturally occurring salt lakes and secondary salinisation from land clearing [*Peters and Donohue*, 2001]. Mean annual discharges into the estuary are variable; the maximum winter discharge rate for the Swan River is 300 m^3s^{-1}, with mean values usually ~100 m^3s^{-1}. Despite this annual variability, the discharge is usually close to zero over late spring to autumn (October to April).

[8] Diurnal tides force the estuary at the seaward boundary (form factor = 3.0 [*Pugh*, 1987]), which is a progressive wave propagating from estuary mouth to station 2 in ~2.5 hours. Diurnal tidal constituents control the forcing, as the semidiurnal amplitudes are small due to the presence of an M_2 amphidromic point within 300 km of the Western Australian coast. Tidal stage is temporally fixed between the austral spring and autumn equinoxes, with low water in the morning and high water in the evening for spring/summer. The reverse occurs during autumn and winter. Mean tidal range is 0.6 m, however, larger anomalies of up to 0.8 m coincide with the passage of atmospheric pressure systems along the Western Australian coastline [*O'Callaghan et al.*, 2007].

[9] The estuary can be divided into upper and lower regions that are delineated by 'The Narrows' (Figure 1). Upstream of this location, the estuary has mostly narrow,

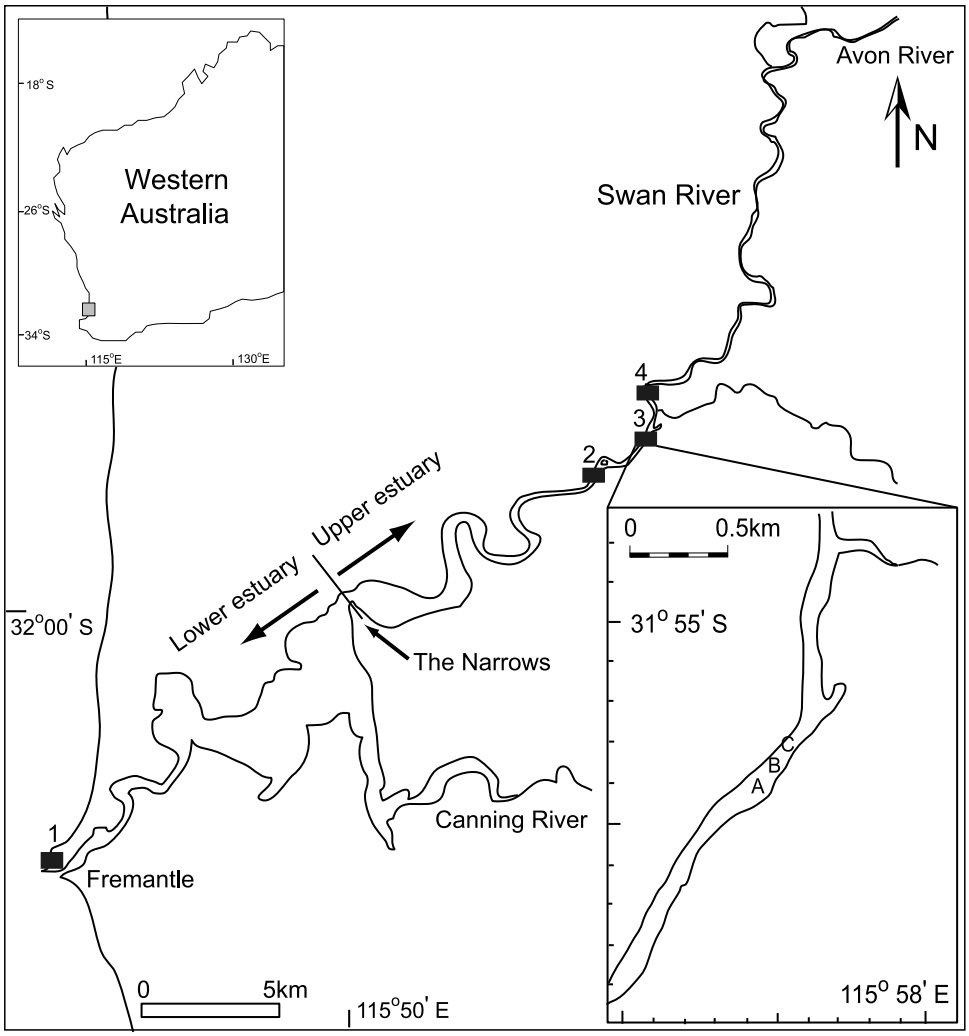

Figure 1. Location map of Swan River estuary, Western Australia, showing sampling stations, major tributaries and delineation of upper and lower estuary. Station details are given in Table 1. The inset in the bottom corner shows instrument sites locations 3A, 3B and 3C for the field experiment during December in 2002.

shallow areas of <100 m wide and 3 m deep, but holes of up to 6 m depth occur at several, irregular intervals to the tidal extent of estuary, some 50 km landward of Fremantle. From November to April the upper estuary has a persistent salt wedge, which is flushed downstream in winter while mixing with water from the lower estuary. In recent years, discharge rates into the estuary have decreased (due to a long-term decrease in the catchment rainfall), and the upper estuary has remained stratified for longer periods of the annual cycle. The lower estuary is marine, with salinity >30 for most of the year [*Spencer*, 1956]; it is 500 to 1500 m wide and has a mean depth of 12 m.

[10] *Hamilton et al.* [2001] used vertical turbidity profiles to interpret suspended particulate matter in the upper estuary near station 2 (Figure 1) over several days. They measured values ranging from 10 to 75 nephelometric turbidity units (NTUs), with peak values observed in the near-bed region. *Hamilton et al.* [2000] suggested the upper estuary, between stations 2 and 4 of this study, was most likely a convergence zone for turbidity akin to the estuarine turbidity maxima observed in higher-energy estuaries [*Uncles*, 2002]. Surficial bed sediments change from sand to fine mud to coarse quartz in the lower, upper, and head of the estuary, respectively [*O'Callaghan*, 2005]. The organic content of bed sediments in the proposed convergence zone is about 10%, but can be more than 30% for suspended sediments at mid-depth in the water column.

3. Sampling Methodology and Analysis

3.1. Data Collection

[11] Data were collected from the upper Swan River estuary in September and December 2001 and December 2002 when daily freshwater discharges were negligible (<2 m^3s^{-1}). Daily discharge data were obtained near the estuary head at Avon-Walyunga (Water and Rivers Commission gauged station no. 616011). The Department of Planning and Infrastructure (DPI, Western Australia) measure tide level data continuously at station 1 and data from

Table 1. Summary of Data Collected in 2001

Station Number	Name	Distance Upstream (km)	Mean Depth (m)	Mean Width (m)	Measurement	Sampling Frequency	Sampling Interval (days)
2001							
1	Fremantle	0.5	15	500	Water level[a]	10-min average	340–365
			9	500	Currents[b]	1 Hz	340–365
2	Ron Courtney	36	3	50	Water level	2-min average	255–270
3	Pickering Park	42	4	80	Turbidity	2-min average	340–350
4	Guildford	45	3.0	50	ADCP	5-min average	342–365
2002							
3A	Pickering Park	42	4	80	Current profiles	0.2 Hz	352–354
3B					Bed currents	8 Hz	352–354
					Turbidity	1 Hz	352–354
3C					Microstructure profiler	10 cms^{-1}	353

[a]Data from DPI.
[b]Data from FPA.

days 244 to 365 in 2001 are used in this study (see Table 1 for sampling details).

[12] Observations reported here can be separated into two categories: mean and turbulent components of velocity, salinity and turbidity. Mean properties were primarily obtained in 2001 and turbulent properties in 2002. Fremantle Port Authority (FPA) supplied the current meter data from station 1 for both sampling periods. These observations are from a single-point S4 current meter moored on a float approximately 3 m from the surface (in 9 m of water). In 2001, two tripods deployed at stations 2 and 3 measured turbidity using a self-cleaning nephelometer [*Ridd and Larcombe*, 1994]. A Nortek AS Aquadopp 2-MHz current profiler was bottom-mounted in a water depth of 4.5 m at station 4. One-minute averages of current velocity were obtained from 400 acoustic pings per minute and were then averaged at five minute intervals. The transducers on this instrument faced upwards to collect current data at 0.2 m intervals from 0.4 to 4.2 m above the bed from days 342 to 365 in 2001.

[13] Mean and turbulent properties of flow, salinity and turbidity were obtained from station 3 in 2002 (sites A, B, and C in bottom inset, Figure 1). A schematic of the sampling approach used at this station is given in Figure 2 to illustrate the different observations being made as the salt wedge oscillates back and forth during the intratidal oscillations. This site, a straight, narrow section of the upper Swan River estuary had minimal lateral flow effects and observations were timed to capture the largest signal-to-noise ratio of the intratidal oscillation. High resolution observations over 42 hours (from days 352.6 to 354.2, 18 to 20 December 2002) were made, again when freshwater discharge was negligible. Wind conditions were calm on days 352 and 353, but by the end of the flood tide on day 353, strong, north-easterly winds were directed upstream along this section of the upper estuary.

[14] At the downstream sampling station, site 3A, a Nortek AS Aquadopp 2-MHz current profiler was bottom-mounted in 3.5 m of water to measure the vertical profile of currents. This instrument has sideways positioned, upward-looking transducers and a thickness of only 0.15 m. Together with a short blanking distance, a much greater proportion of the water column was captured with the first bin located 0.4 m from the bed. Vertical profiles were collected in 0.30 m bins to the surface and currents were burst sampled as 1-minute averages every 5 minutes.

[15] At site 3B, a Chelsea Instruments nephelometer and a Nortek AS 6-MHz vector were mounted on an autonomous tripod, which was deployed for 38.5 hours from days 353 to 354. The vector is an acoustic current meter that measures three-dimensional flow components (u, v, w) at a frequency of 8 Hz, allowing instantaneous currents to be resolved for determining turbulence. Observations related to a water parcel diameter and height of 15 mm, about 0.25 m above the bed. The Chelsea nephelometer was housed and powered by the analog channel of the vector, sampling turbidity at a frequency of 1 Hz. Pressure data were also sampled at 1 Hz by the vector. All parameters were burst-sampled, and 18-minute bursts were logged to internal memory every 30 minutes.

[16] Vertical profiles of temperature and conductivity were obtained with a conductivity-temperature (CT) microstructure profiler (SCAMP) [*Stevens and Smith*, 2004] approximately every 10 minutes on the flood tide on day 353 at site 3C. The depth and width of the estuary at this site is 4.5 m and 100 m, respectively. The CT profiler was released at the surface and allowed to free-fall at a nominal rate of 0.1 m^{-1}. Two combined CT sensors are mounted close to each other and protrude from the front of the profiler, allowing calculation of fine-scale gradients of temperature based on the spatial differences. The profiler was

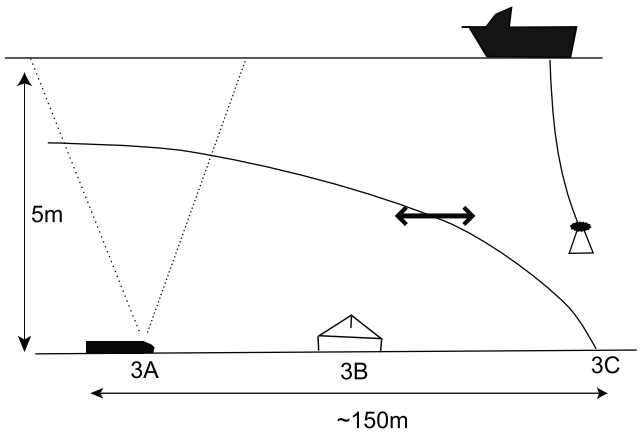

Figure 2. A schematic of the sampling approach used at station 3 in 2002 showing the observations being made as the salt wedge oscillates back and forth during the intratidal oscillation.

also equipped with a pressure sensor to measure the depth. The temperature, conductivity, and pressure sensor resolutions were 6×10^{-4} °C, 2×10^{-2} S m^{-1} and 2×10^{-2} m^{-1}, respectively. Each sensor was calibrated prior to deployment.

3.2. Data Analysis

[17] Harmonic analysis using TIRA (Tidal Institute Recursive Analysis) determined the amplitude and phase of the tidal constituents from the water level records [*Pugh*, 1987]. The analysis was also performed on the east-west and north-south current components. The estuary orientation at each station was used to resolve the currents into their axial and lateral components. Only the axial components are included here, as the narrow (mostly <100 m) upper estuary meant that the lateral effects were negligible. Detrending the time series and removal of mean velocities per burst were used to resolve the high resolution instantaneous current data into the dimensional turbulent fluctuations (u′, v′, and w′) from the deviation of the mean or the Reynolds decomposition [*Tennekes and Lumley*, 1994]

$$u'(t) = u(t) - \overline{u} \qquad v'(t) = v(t) - \overline{v} \qquad w'(t) = w(t) - \overline{w}. \quad (1)$$

Bed shear stresses (τ, Nm^{-2}) were calculated directly from the Reynolds stresses as:

$$\tau = \rho\overline{\mathrm{u'w'}}. \quad (2)$$

An indirect method outlined by *Dyer et al.* [2004] was also used to estimate τ from the turbulent kinetic energy (TKE) as

$$TKE = \frac{1}{2}(u' + v' + w')^2 \quad (3)$$

$$\tau = 0.19\rho\mathrm{TKE}, \quad (4)$$

where u′, v′, and w′ are the turbulent fluctuations of u (east-west component), v (north-south component), and w (vertical component), respectively, and ρ is the water density.

[18] Reynolds stresses used the 8-Hz current data from the vector and each detrended 18-minute burst was resolved as turbulent fluctuations from the mean. This method is more sensitive to instrument orientation than using turbulent kinetic energy (TKE) to determine the shear stress [*Dyer et al.*, 2004]. Reynolds fluxes are the cross product of the turbulent variations in vertical/horizontal velocity and turbidity concentrations, i.e., w′c′ or u′c′. The averaged Reynolds fluxes represent the turbulent transport of suspended material in either the horizontal or vertical directions [*van der Ham et al.*, 2001; *Dyer et al.*, 2004]. These data had different sampling frequencies (8 Hz for instantaneous flow compared with 1 Hz for turbidity) so velocity data were averaged to 1 Hz, then the Reynolds flux was estimated for each burst.

[19] The backscatter or echo intensity (E) from the acoustic signal strength of the acoustic Doppler current profiler (ADCP) was used to calculate the echo level (EL) [*Deines*, 1999]. The EL indicates the volume of scattering particles in the water column and provides an indirect estimate of the suspended particulate matter (SPM). The EL measurements were not calibrated with concentrations of suspended matter as the observations of EL were for comparative purposes only. Studies in other estuaries have shown that there is a high correlation between EL and in situ suspended matter concentrations [*Hoitink and Hoekstra*, 2005; *Kim and Voulgaris*, 2008].

4. Results

[20] Four main constituents, K_1, O_1, M_2, and S_2, in order of decreasing contribution controlled diurnal tidal variability at stations 1 and 4. Despite the Swan River estuary being characterized as having a diurnal tide [*Hodgkin and Di Lollo*, 1958], our observations found that: (1) the tidal frequency actually varied throughout the year with a clear diurnal signal closest to the solstice that became more semidiurnal near to the equinox; (2) repeated intratidal oscillations occurred over a 24-hour tidal cycle, with the highest magnitude observed close to the solstice when the tides were predominantly diurnal. These findings provide the framework for the following results.

4.1. Tidal Phase Variability

[21] Tidal curves were reconstructed for each of the four main constituents for comparison using the following:

$$a(t) = \sum_N H_n \cos(\omega_n t - g_n). \quad (5)$$

Where a is the amplitude, H_n and g_n the amplitudes and phases of the tidal constituent and ω_n the angular frequency of the constituent.

[22] Diurnal (K_1 + O_1) and semidiurnal (M_2 + S_2) tidal curves from station 1 based on their respective amplitudes and phases are shown in Figure 3a. The resultant tide based on the summation of these four tidal curves follows in Figure 3b. The larger amplitude oscillations with range 0.6 m represented the diurnal tide while the semidiurnal tide produced smaller oscillations of only 0.2 m. As expected from tidal theory, tidal ranges from the semidiurnal tide were related to the lunar cycle, with maximum tidal ranges occurring close to full and new moons (days 289 and 306), and minimum tidal ranges occurring close to the first and last quarters of the lunar cycle (days 297 and 310, Figure 3a). However, the diurnal tidal range did not always correlate with lunar stages. For example, a tidal range of only 0.2 m occurred with the full moon on day 289 (Figure 3b). This difference for diurnal tides was a result of the tropic month having a shorter period than the synodic period (27.6 days compared to 29.5 days).

[23] Definitions of spring and neap tides state that tidal ranges are tied to the lunar stage (definition of spring tide from Merriam-Webster Online Dictionary, retrieved 3 March 2010, available at http://www.merriam-webster.com/dictionary/spring tide). Spring tides occur at, or soon after, the new and the full moon and have a maximal tidal range, whereas minimum (or neap) tidal range occurs during the second and fourth quarters of the moon [e.g., *Dyer*, 1997; *Pugh*, 2004]. Therefore, the terminology of spring and neap tides is inaccurate in diurnal systems and are defined as tropic and equatorial tides herein. For tropic tides (analogous to spring tides for semidiurnal systems) the tidal range is a maximum when the declination of the moon is

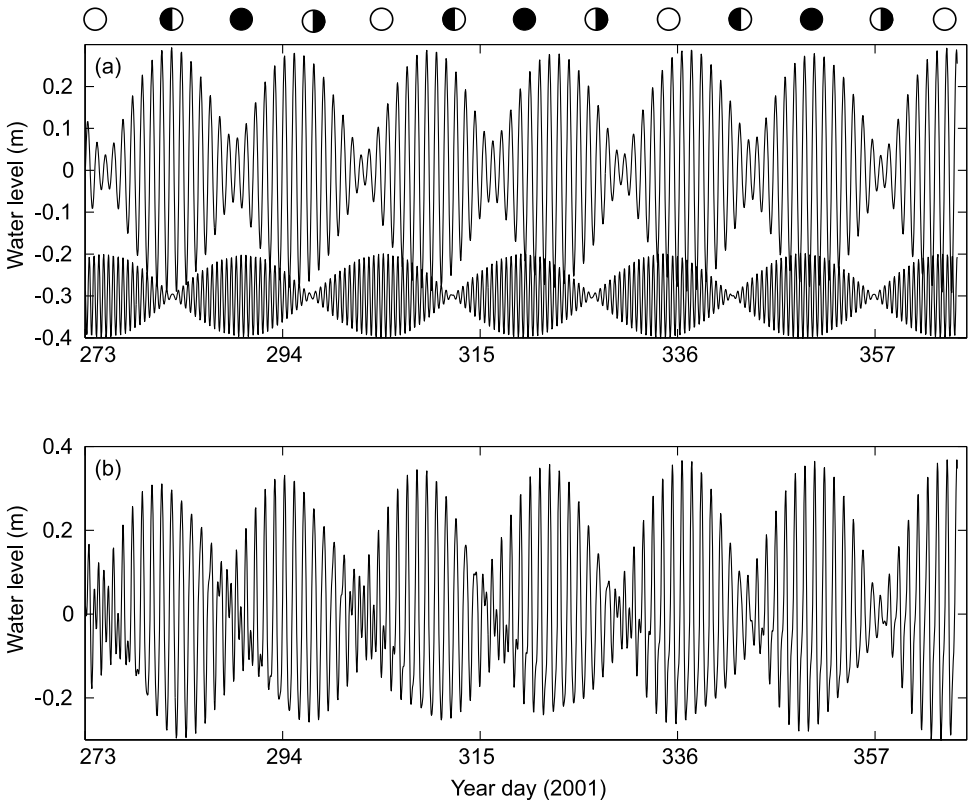

Figure 3. (a) Diurnal and semidiurnal inputs to the tide from day 273 (October 1) to day 365 (December 31) in 2001. (b) Water level from the summation of the diurnal and semi-diurnal constituents. Phases of the moon are included above the upper axis.

north or south of the equator. For equatorial tides (analogous to neap tides for semidiurnal systems) the moon is directly above the equator resulting in a low tidal range.

[24] A phase difference over an annual cycle resulted from the diurnal and semidiurnal tides oscillating at a frequency of 13.63 and 14.77 days, respectively (Figure 3b). Three regimes are manifested from this difference, with diurnal and semidiurnal tides either in-phase, out of phase, or time-lagged that corresponded to the solstice, equinox, and remainder of the year, respectively. In-phase signals produced a maximum tidal range and a strongly diurnal tide; out-of-phase signals produced a minimum tidal range yet still with 24-h period. At any other time the tide had a mixed frequency with intermediate tidal ranges. Mixed tides occurred mostly during equatorial tides closest to the equinox (day 275, Figure 3b), with two high waters and low waters usually observed over a 24-hour diurnal tidal cycle. Near the summer solstice (day 351, Figure 3b), the diurnal and semidiurnal tidal inputs were aligned almost identically to those of diurnal systems; that is, the largest diurnal tidal range (tropic tide) occurred with the largest semidiurnal tidal range, producing the largest tidal range of any fortnightly cycle. Over the three months (September to December 2001), the maximum tidal ranges increased from 0.6 to 0.9 m, as the moon's orbital plane oscillated from a minimum to maximum declination angle.

[25] Variability in tidal currents was attributed largely to tidal behavior at the mouth of the estuary. Seven days of current data from station 1 (in 2001) showed the response near to the equinox (days 295 to 302, Figure 4a) and solstice (days 350 to 357, Figure 4b). Over the seven day spring to neap period near the equinox (minimum tidal range), the ebb asymmetry weakened and by day 301 the duration of the flood and ebb tides was almost identical. Current speeds almost halved over this time, from 0.6 to 0.35 ms^{-1}. Near the solstice (maximum tidal range) currents also decreased substantially over the 7-day period (days 350 to 357), but the ebb-dominant asymmetry persisted and by day 357 the maximum currents on the ebb tide were approximately twice those of the flood tide. A 25% increase in current speeds was evident from September to December, and corresponded to a rise in the mean tidal range associated with the transition from the equinox to the solstice. Of particular note was the rapid change in tidal currents early in the flood tide at the ocean boundary (clearest for day 350 and 351, Figure 4b).

4.2. Intratidal Oscillation

[26] Intratidal oscillations, defined here as a change in the rate of water level increase or decrease ($d\zeta/dt$) during the flood tide, were observed in the lower and upper estuary with amplitudes of less than 0.1 m. Strongest intratidal oscillations occurred nearest to the solstice when tides were strongly diurnal and the tidal range was greatest. The duration of these oscillations was typically 2 to 3 hours. Summation of the tidal constituents, obtained from harmonic analysis of water level data, indicated that all four constituents, K_1, O_1, M_2, and S_2 contributed to the formation of intratidal oscillations (Figures 5a and 5b). At

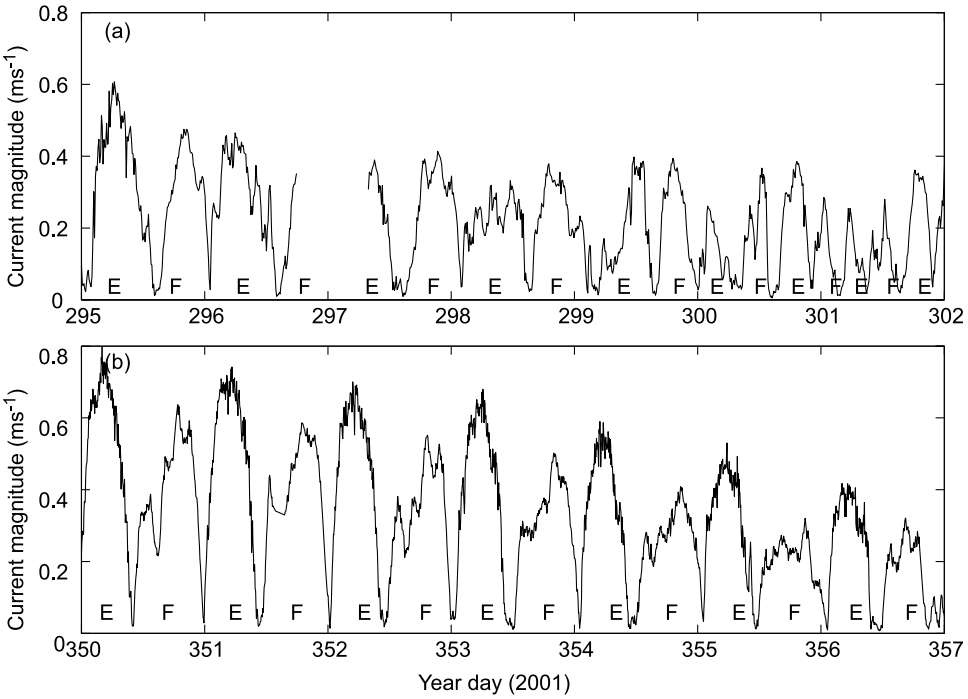

Figure 4. Current magnitudes from station 1 at 3 m below the free surface for (a) days 295 to 302 and (b) days 350 to 357 in 2001. The start of each time series corresponds to the tropic for October (Figure 4a) and December (Figure 4b) in 2001. E and F indicate the ebb and flood-tide, respectively.

stations 1 and 4, the K_1 constituent made the largest contribution to the resultant tide, with a 3-hour lag between these two stations. Attenuation of the diurnal and semidiurnal constituents were around 50% and 40%, respectively, between stations 1 and 2 (data not shown).

[27] Short-term variability of the vertical current profile was associated with the intratidal oscillation. Vertical profiles of axial currents on the ebb tide had an almost logarithmic profile directed downstream, with near-bed speeds of 0.05 ms^{-1}, that increased to 0.2 ms^{-1} near the surface (Figure 6). Just prior to low water, the vertical profile became two-layered with flow in the lower 1.8 m of the water column directed upstream at approx. 0.05 ms^{-1}. By the start of the flood tide flow was more vertically uniform, with speeds c. 0.2 ms^{-1} from the bed to the surface and directed in to the estuary. The intratidal oscillation was characterized by very weak currents, around an order of magnitude smaller, in the lower 2 m of the water column almost 3 hours after low water (LW + 3, Figure 6). Five hours after low water (LW + 5, Figure 6), current speeds increased to 0.2 ms^{-1} and the vertical profiles were again almost uniform. This non-localized response of decreasing current speeds during mid-flood was also observed at station 1 (Figure 4b). Since these latter observations were from a single-point current meter located 3 m from the surface comparisons of vertical variability between the lower and upper estuary could not be made.

4.3. Destratification During the Flood Tide

[28] The evolution of density structure and flow dynamics during an intratidal oscillation were examined in more detail using observations from a subsequent field campaign in 2002. Intensive sampling over a single ebb and flood tide on day 353 (Figure 7) showed an enhancement of stratification and then subsequent destratification over a 2 to 3 hour window coincident with the intratidal oscillation. Initially the tide ebbed from 00:00 to 10:00 h, with low water at 10:18 h. Nearly 2.5 hours after low water (~12:30 h) water level decreased for 2 hours until 14:27 h corresponding to the end of the intratidal oscillation. Water level continued to increase for the remainder of the flood tide until high water close to c. 23:00 h. A highly variable $d\zeta/dt$ was evident for the flood tide, with a localized minimum at the end of the intratidal oscillation around 14:30 h (Figure 7). This was in contrast to the near monotonic increase in $d\zeta/dt$ over the ebb tide.

[29] Destratification of the near-bed halocline occurred early in the flood tide on day 353 (Figure 8). The halocline was located between 3 and 3.5 m deep from ~12:00 to 13:30 h and had a top-to-bottom salinity difference (ΔS) of 3.5 during the intratidal oscillation (compared to ΔS of 3 at low water). The water column began destratifying from 13:30 h, and ΔS then decreased to 0.3 for several hours. Near- to well-mixed conditions persisted for ~1.5 hours, from 14:30 to 16:00 h, after which time bottom salinity and ΔS increased again with strengthening stratification later in the flood tide.The squared buoyancy frequencies were calculated using

$$N^2 = \frac{-g}{\rho_o}\frac{\partial \rho}{\partial z}, \tag{6}$$

where N is the vertical buoyancy frequency, g is the gravitational acceleration, ρ is the density, ρ_o is a constant reference density, and z is the depth. The depth-averaged buoyancy frequency (N) was initially 0.077 s^{-1} at low water

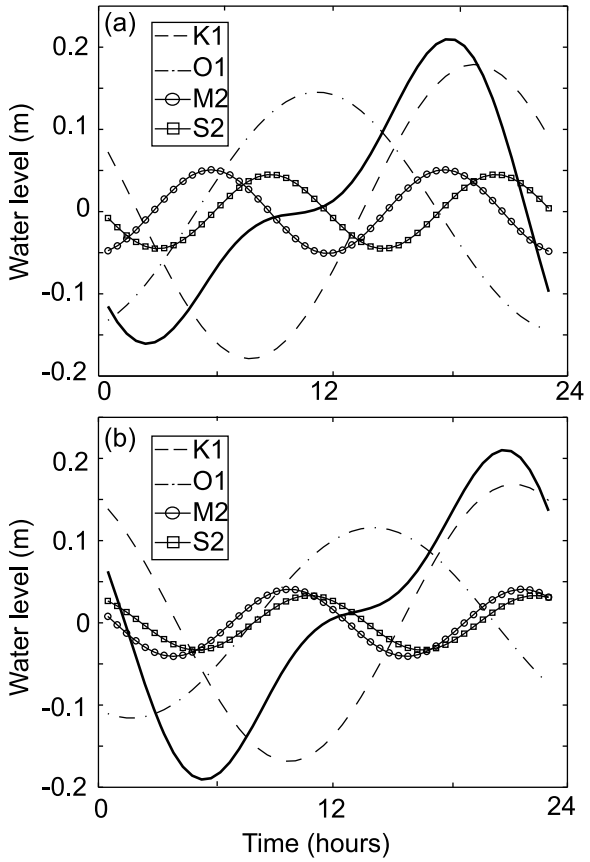

Figure 5. Individual tidal curves of the four main constituents at (a) station 1 and (b) station 4. The resultant tidal curve (continuous solid line) is the summation of these four constituents.

(~1000 h). For the period of strongest stratification after low water, N was only slightly larger at 0.0818 s^{-1}. By reducing ∂z to the pycnocline thickness (of ~1 m) estimates of N were an order of magnitude larger (0.136 s^{-1}). Near to the end of the flood tide vertical density gradients were relatively weak and N had decreased to 0.04 s^{-1}. These values were similar to those found in other partially mixed estuaries [*Becker et al.*, 2009] while the larger N values are similar to those observed across the halocline in the highly-stratified Hudson River [*Peters*, 1997].

[30] Critical times for shear-induced mixing were identified by examining coincident vertical profiles of axial currents and salinity on day 353. At low water (Figure 9a) the characteristic two-layer estuarine flow was present, with strong vertical stratification. At 13:27 h, the halocline c. 1 m from the bed, delineated upstream and downstream flows (Figure 9c). Above the halocline, currents were directed upstream at 0.1 ms^{-1} while below the halocline, the currents were weaker and oriented downstream. By 14:27 h, both currents and salinity were essentially uniform in the vertical (Figure 9d). Over the one-hour period (from 13:27 to 14:27 h), the water column changed from being strongly stratified to almost well-mixed conditions, which persisted until 16:21 h. After this time both bottom salinity and currents increased again. During the flood tide the strongest currents (0.2 ms^{-1}) occurred in the near-bed region at 18:10h (Figure 9h), while at the same time the lowest sub-surface currents were observed, a complete reversal to the vertical current profile shown in Figure 9b.

[31] Repeated SCAMP profiles of density and temperature gradients (dT/dz) over the flood tide were used to determine the physical locations of turbulent mixing [*Lemckert et al.*, 2004] during periods alternating between stratification and destratification (Figure 10). Early in the flood tide (10:50 h, Figure 10a), stratification across the pycnocline region (2.3 to 3 m water depth) was moderate with σ_t ($\sigma_t = \rho - 1000$) spanning 1.0 kgm^{-3}. Weak turbulent mixing was present along the pycnocline and in the surface layer as reflected in the vertical temperature gradients < ± 5 °Cm^{-1}. Wind stress was likely to have caused the gradients/mixing near to the surface layer.

[32] Figure 10c (13:27 h) was considered to define the start of the intratidal oscillations. At this time, there was a

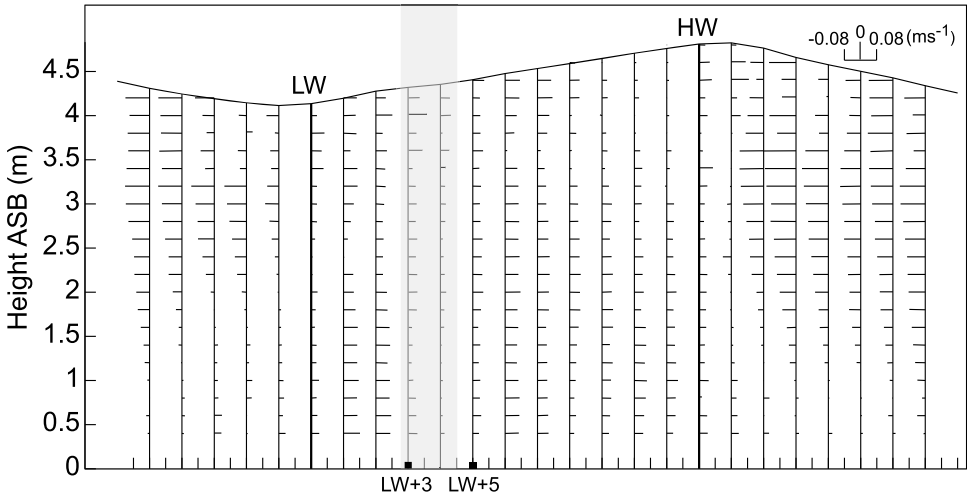

Figure 6. Vertical current profiles above sea bed (ASB) from station 4 over 25 hours on day 349 in 2001. LW = low water; HW = high water; LW + 3 = low water plus three hours; LW + 5 = low water plus five hours. The shaded area highlights the current's response during the intratidal oscillation.

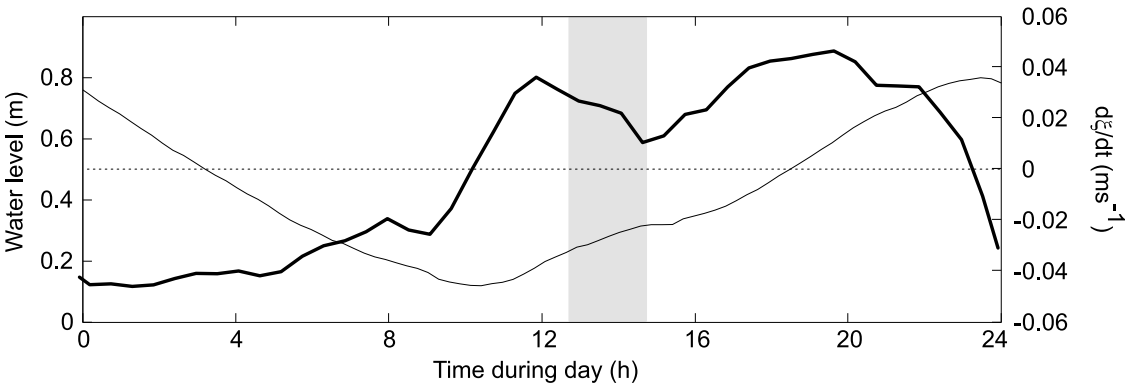

Figure 7. The water level (thin line) and water level gradient (thick line) over 24 hours on day 353 in 2002. The dotted, horizontal line indicates zero crossing for the time derivative of the water level, and the shaded area highlights the timing of the intratidal oscillation.

sharp pycnocline and σ_t of ~1.8 kgm^{-3}, almost double that observed in the early part of the flood tide. An unstable density profile at 3 m, i.e., a higher density parcel of water overlying less dense water, was coincident with a strong dT/dz (± 15 °Cm^{-1}) that was three times higher than at 10:50 h. One hour later (14:27 h, Figures 10e and 10f), the water column was almost homogenous from the surface to within 0.4 m of the bed. The density in the lower 0.4 m was unstable and turbulent mixing was evident as denoted by high variations in the temperature gradient signal of up to ± 18 °Cm^{-1} in the near-bed region. Later during the flood tide, approximately seven to eight hours after the intratidal oscillation had occurred, the density and dT/dz profiles (Figures 10g and 10h) indicated moderate restratification (σ_t <1.0 kgm^{-3}) and weak temperature gradients similar to those at the start of the flood tide.

[33] Reduction of the gradient temperatures profiles to turbulent energy dissipation rates, ϵ, were completed using the stationary segment method described by *Imberger and Ivey* [1991]. The method consists of fitting an auto-regressive model to two adjacent windows (a size of 256 samples was used here) of the data corresponding to the temperature gradient. The resulting coefficients are used to estimate the distance between the two data sets (as a norm). Fast Fourier transform analysis is performed on each segment to provide estimates of dissipation of turbulent energy [*Etemad-Shahidi and Imberger*, 2002]. A threshold of 10×10^{-10} m^{2}s^{-3} excluded nonactive segments. In some cases it was not possible to fit the Batchelor spectrum to the data and when this occurred the segment was left blank. An example from the most active profile at 14:27 h is shown in Figure 11. The highest value of ε for the four profiles Figures 10a–10h was 9×10^{-4} m^{2}s^{-3} in the near-bed region. It was an order of magnitude greater than the surface ε values of 8.8×10^{-5} m^{2}s^{-3} that were most likely caused by weak surface wind mixing.

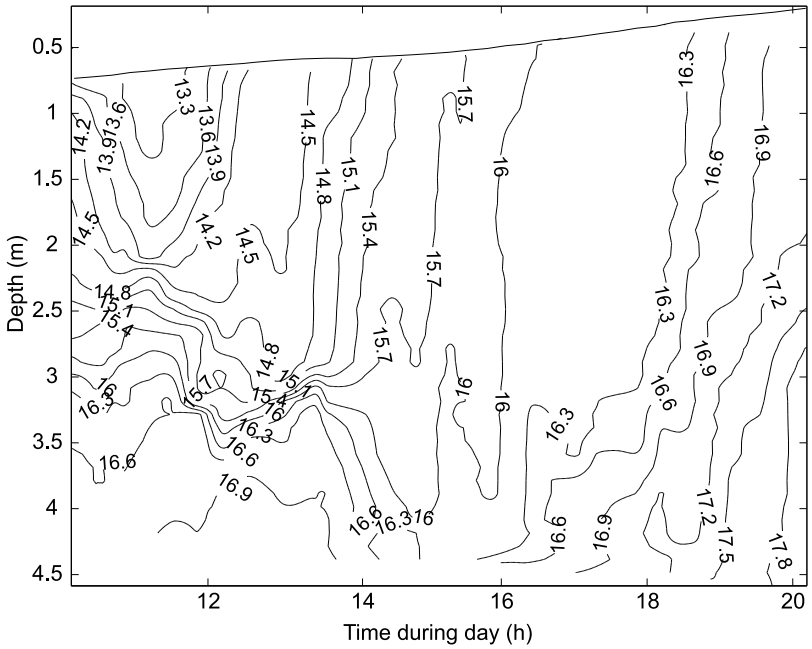

Figure 8. Salinity contours over the flood tide on day 353 in 2002.

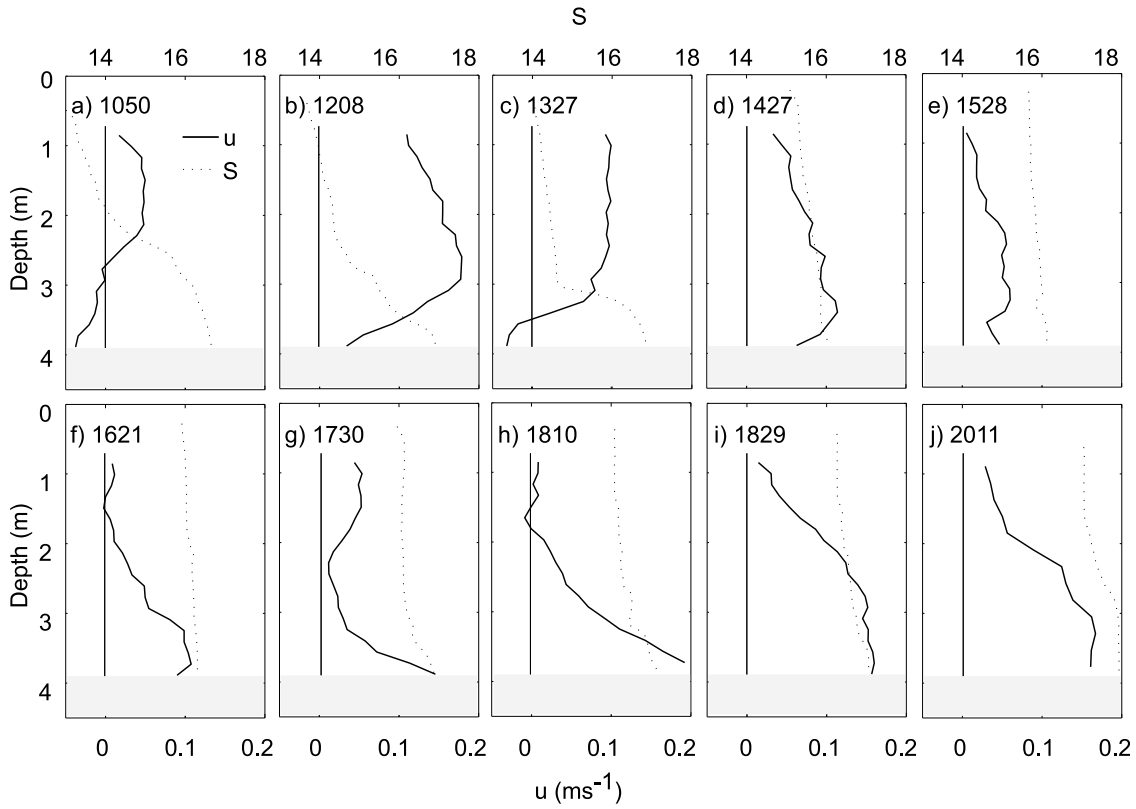

Figure 9. Vertical profiles of along-river currents (thick line) and salinity (dotted line) at approximately one-hour intervals for 10 hours over the flood tide. Positive and negative velocities are directed upstream and downstream, respectively. The vertical line indicates the zero crossing between upstream and downstream flow. The time of each profile is shown in the top left corner.

4.4. Sediment Response to the Intratidal Oscillation

[34] Sediment entrainment and resuspension occur when bed stresses (from mean current velocities) exceed critical erosion thresholds based on local sediment composition. In estuaries, this stress is induced by the flow near the bed that is forced by tides, surface waves and/or freshwater inflow. In the absence of significant surface waves and freshwater inflows to induce resuspension and with low near-bed velocities (<0.1 ms^{-1}), a relatively 'quiescent' hydrodynamic regime would be expected to prevail in the Swan River estuary. Sediment resuspension and transport would mostly likely be during high freshwater inflows which are limited to a few months of the year. However, increased and regular turbidity events occurred at the upper most station (station 4) over a 17-day period (Figure 12). Maximum backscatter peaks of 60 dB (at 1 m from the bed) coincided with intratidal oscillations over the tropic tide from days 361 to 363 (Figure 12). Slightly smaller, cyclical variations in backscatter were also present for the earlier tropic tide (day 350 to 353). Near-bed velocities were consistently close to zero (within the measurement error of the instrument) for each ebb tide. Current speeds increased away from the bed to a maximum velocity of 0.2 ms^{-1} at the surface and were directed seawards on the ebb (Figure 12b). On the flood, however, current directions varied from initially upstream, to downstream, and finally upstream again. Magnitudes fluctuated from ± 0.1 ms^{-1}. Of most interest for understanding the physical controls on sediment concentrations was the reversal of the weak currents during the intratidal oscillations.

[35] Observations from station 3, again, captured repeated turbidity peaks over the fortnightly cycle at station 3 using self-cleaning turbidity meters (Figure 13a). Repetitive peaks in excess of 200 NTU were observed over 11 consecutive flood tides. These large spikes in turbidity were concentrated over the tropic tide. The timing of peaks became more variable closer to the equatorial tide near days 357 to 360. Each turbidity peak (up to 250 NTU) typically lasted for only around two hours before decreasing to c. 25 NTU. Concentrations of suspended particulate matter, in the water column, for the 2 to 3 hour duration of an intratidal oscillation ranged from 40 to 55 mgL^{-1} at station 3 [*O'Callaghan*, 2005]. Turbidity did not usually exceed 40 NTU for the remainder of the tropic tide, and tended to be low throughout the equatorial tide, with one exception when turbidity reached 260 NTU for around 30 minutes on day 357. This anomaly was also present at station 4 (Figure 12c).

[36] The frequency of the intratidal oscillation was once every tidal cycle and characterized by the relatively static water level for 2 to 3 hours on the mid-flood tidal stage (Figure 13b). But within a single tidal cycle (and intratidal oscillation) multiple turbidity 'spikes' with durations of up to 40 minutes were observed. Turbidity amplitudes for each of the 3 days (347 to 350) were similar, although the timing varied for the three intratidal oscillations. A similar

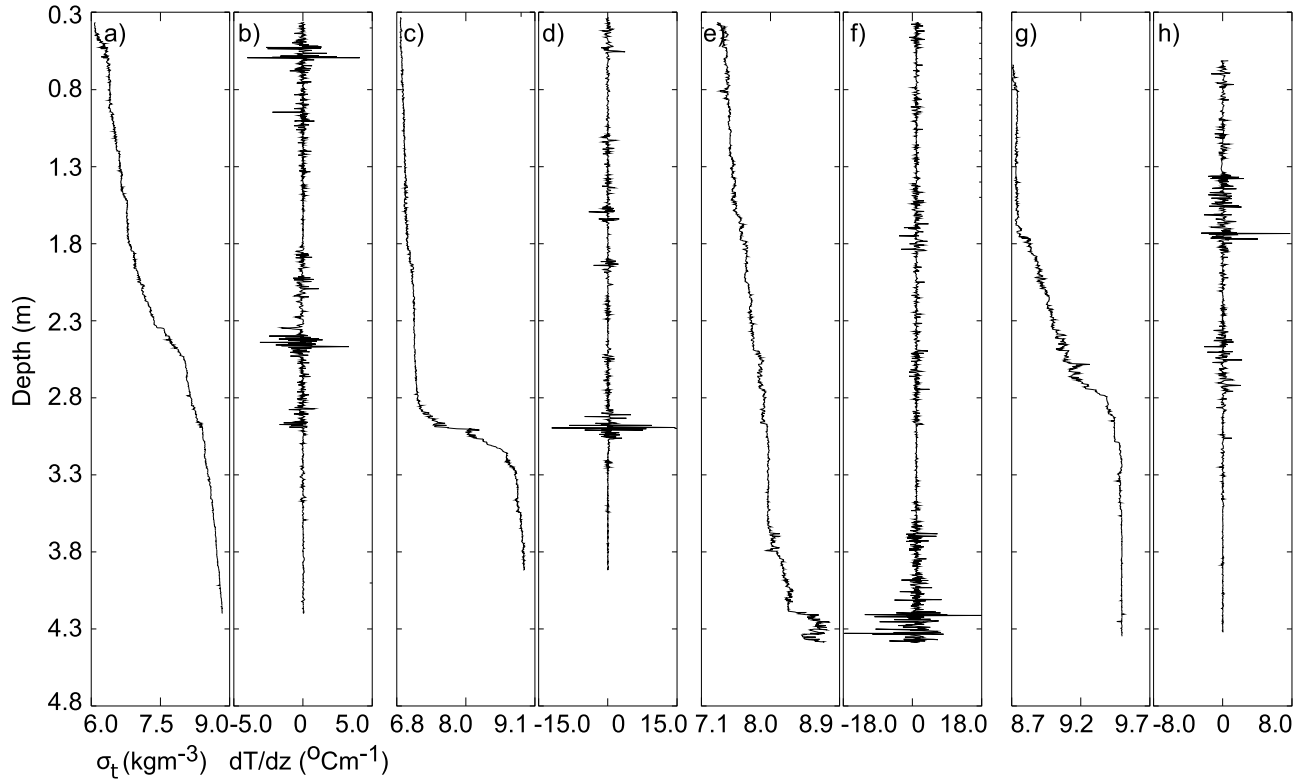

Figure 10. Vertical profiles of stratification (σ_t) at (a) 10:50, (c) 13:27, (e) 14:27, and (g) 20:11. (b, d, f, and h) Profiles of the gradient temperature at corresponding times are shown. Note that the σ_t (stratification) and dT/dz (temperature gradient) values are different for Figures 10a–10h to preserve the features of each profile.

response - multiple peaks during the intratidal oscillation - was observed at station 2, albeit with reduced turbidity peaks.

[37] Bed shear stress, τ_o, was calculated using the quadratic stress law, $\tau_o = C_D U^2 \rho$, where C_D is the drag coefficient of the bed and is 3.1×10^{-3}, U is the mean current velocity, and ρ is the water density of ~1007 kgm^{-3} [*van Rijn*, 1989]. The bed shear stress (τ_o) at 1 m from the bed ranged between 0 and 0.03 Nm^{-2} on day 349 (Figure 14). Using methods outlined by *Mitchener and Torfs* [1996], a critical erosion threshold (τ_{cr}) was estimated, for the Swan River estuary, based on sediments having a combined mud/sand composition and a bulk sediment density of 1150 kgm^{-3} [*O'Callaghan*, 2005]. This τ_{cr} value was 0.55 Nm^{-2} and much higher than in situ estimates of between 0.08 to 0.12 Nm^{-2} from Chesapeake Bay, for similar sediment types [*Wright et al.*, 1997]. Nevertheless, there was no instance over the tidal cycle when τ_o exceeded either estimate of τ_{cr} from the Swan River or Chesapeake Bay.

[38] Using observations from 2002, we examined near-bed turbulence characteristics during the flood tide on day 353. Estimates of bed shear stress (τ) from the Reynolds stress and TKE methods ranged from 0.5 to 3 Nm^{-2} (Figure 15a). *Dyer et al.* [2004] discussed a critical threshold (τ_{cr}) for active turbulence, i.e., the energy required for sediment mobilization from the bed, as τ_{cr} >0.2 Nm^{-2}. This value provided the lower critical threshold in Figure 15a, and the earlier τ_{cr} of 0.55 Nm^{-2} derived from Swan River estuary sediments specified the upper limit. Bed stresses from the Reynolds stresses (or direct method) exceeded both values of τ_{cr} near 18:00 h for ~2.5 hours and again for a further hour at 22:00 h. Whereas mobilization of bed sediments estimated from the TKE stresses (or indirect method) occurred several times during the flood tide: immediately after low water, at the end of the intratidal oscillation, and from 18:00 h onwards.

[39] Extracting time series of backscatter allowed us to determine Reynolds fluxes in the horizontal and vertical directions (Figures 15b and 15c). Large vertical fluxes were evident from 16:00 to 21:00 h, which physically translated to an upward-moving fluid parcel of high turbidity (or material). Of particular interest, for understanding the anomalous intratidal oscillations, were the negative Reynolds fluxes at 14:00 h indicating transfer of material towards the bed. By considering changes in the horizontal/vertical flux ratio (u′c′/w′c′) over the flood tide, regions where turbulence is generated can be identified [*van der Ham et al.*, 2001]. This ratio was slightly greater than 1 near to the intratidal oscillation and suggests this turbulence was generated at mid-depths of the water column. Later in the flood tide, the ratio increased up to 3.5 (by 18:00 h) and demonstrates the anisotropy of near-bed turbulence.

5. Discussion

[40] With fewer investigations in low-energy estuaries, our understanding is limited of how the competing processes of advection, stratification and mixing interact in these

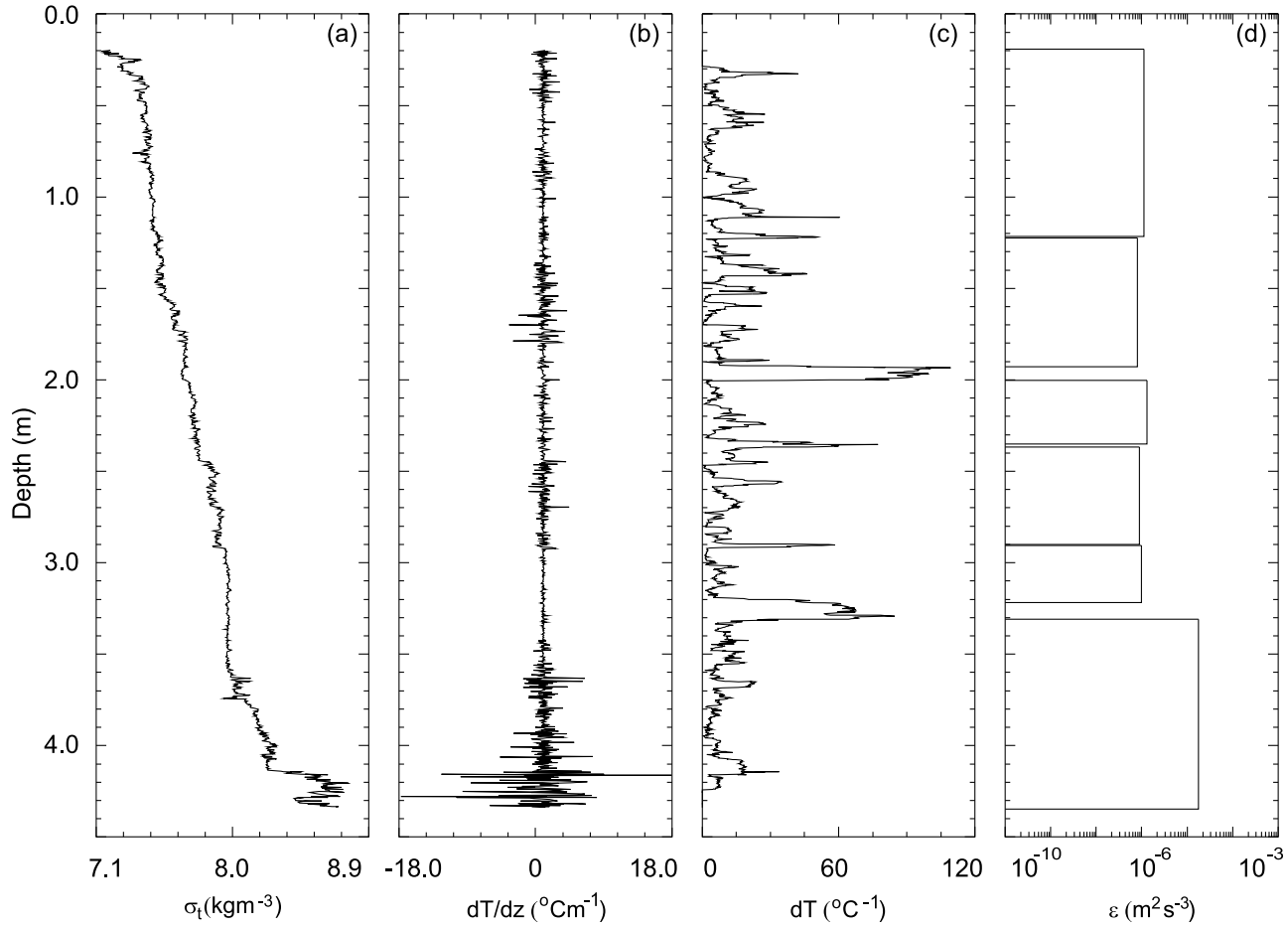

Figure 11. Vertical profiles of (a) σ_t, (b) temperature gradient profile, (c) norm distance computed using autoregressive models, and (d) dissipation of turbulent kinetic energy per segment (ϵ) at 14:27 h.

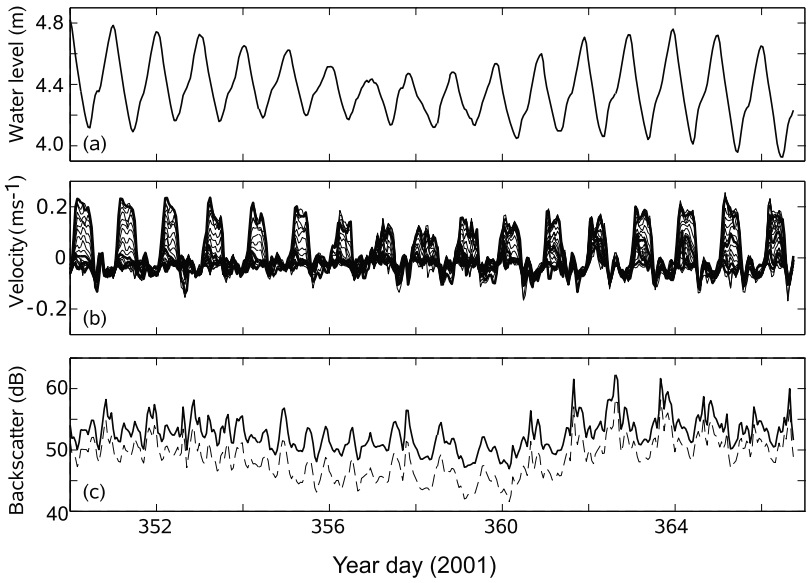

Figure 12. Time series of (a) water level, (b) tidal currents for each vertical bin from 0.4 m above the bed to near surface, and (c) acoustic backscatter 1 and 2 m from the bed for a 17-day period in 2001.

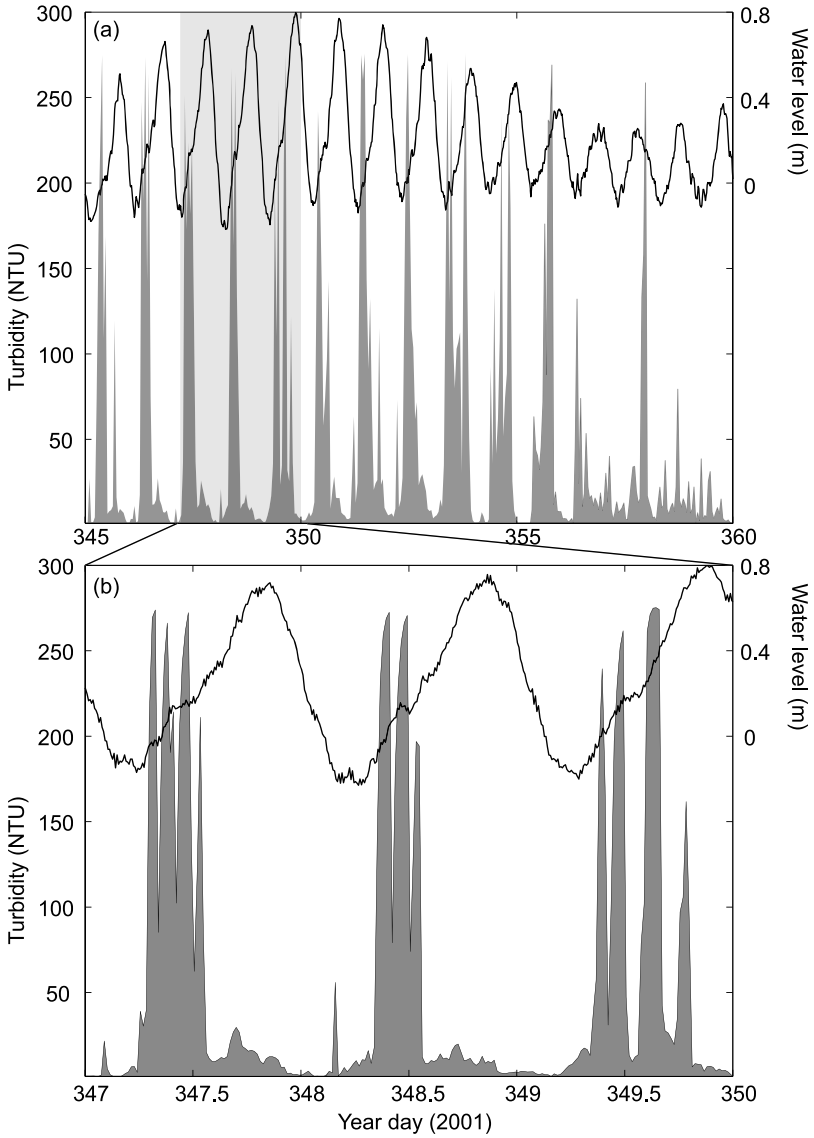

Figure 13. The water level (station 4) and turbidity (station 3) for (a) days 345 to 360 and (b) days 347 to 350, a subset of data in Figure 13a, in 2001.

systems. Using observations from the Swan River estuary we were able to characterize diurnal tidal variability at the fortnightly and 24-hour tidal frequency. Analysis of progressively shorter timescales allowed us to focus on understanding the transport mechanisms generated by mean and turbulent physical processes.

5.1. Behavior of the Diurnal Tide

[41] Astronomical forcing rather than shallow water distortion causes tidal asymmetry in diurnal tidal systems [*Ranasinghe and Pattiaratchi*, 2000]. This forcing varies seasonally as the lunar and solar systems oscillate through their respective cycles. With the main semidiurnal astronomical constituents having frequencies near to the first harmonics (K_2, O_2) of the two main diurnal constituents, contributions from these are masked. Accordingly, the common relationship between the dominant constituent and its harmonic (M_2/M_4 [*Aubrey and Speer*, 1985] that controls asymmetry is relatively insignificant in a diurnal system, i.e., the K_1/K_2 ratio.

[42] Observations from another mixed, mainly diurnal system (Red River Delta [*van Maren et al.*, 2004]) showed that the interactions of K_1, O_1 and M_2 lead to a cyclic asymmetry with a spring tide maximum over a half-year period. However, we found that the amplitude and phase of the four main constituents, K_1, O_1, M_2, and S_2, are required to replicate water level observations in the Swan River estuary. Removal of the S_2 constituent to compare to the analytic method outlined by *Hoitink et al.* [2003] led to under resolved spring-neap cycles near to the summer solstice. Moreover, intratidal oscillations are absent when S_2 contributions are not included in tidal reconstructions. Several distinctions exist between this system and that described by *van Maren et al.* [2004]. Not only is the size of the Swan River estuary vastly smaller than the Gulf of Tonkin in Vietnam, but the amplification of the M_2 constituent by wave reflection in the shallower bay region of the

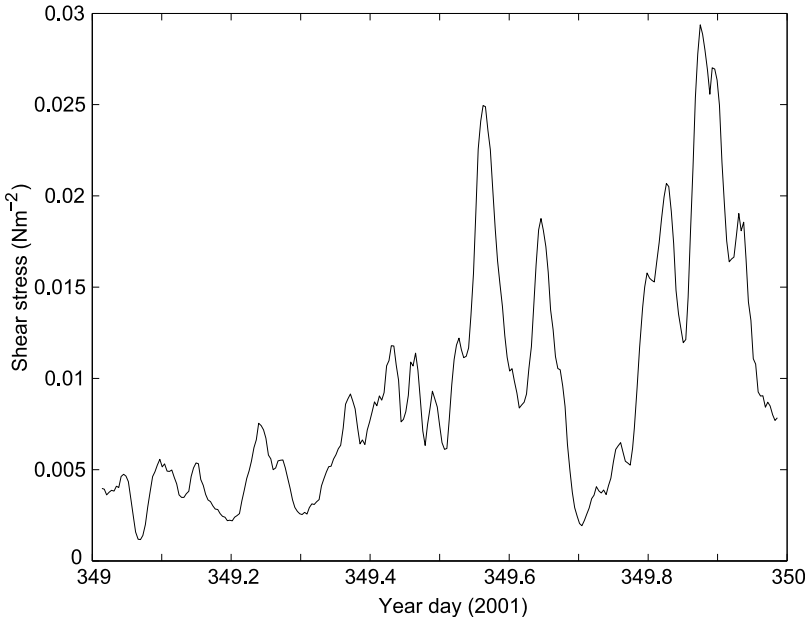

Figure 14. Bed shear stress at station 4 for day 349 in 2001 determined using the quadratic stress law [*van Rijn*, 1989].

Gulf leads to a dominance of semidiurnal constituents. Attenuation of the main semidiurnal constituents (and also diurnal constituents) is uniform along the length of the Swan River estuary maintaining the need for S_2 contributions in the upper and lower regions.

[43] The strongest intratidal oscillations near to the Austral summer solstice last for 2 to 3 hours on the flood tide. At the onset of the flood tide velocity decreases, then is weak and stable for the duration of the intratidal oscillation, but with increasing water level pre-intratidal oscillation speeds return in the late flood. The rate at which the currents increased after the intratidal oscillation was similar to that observed in the change from low water to flood tide. Despite similar accelerations over the tidal cycle and low current speeds during the intratidal oscillation, turbidity events occur at this time on the flood tide. The only comparable tidal phenomenon was found in Southampton Water, UK, which also experiences an unusual tidal phenomena: the 'young flood stand'. At mid-flood, water level has a static phase, at that location, for ~2 hours [*Levasseur et al.*, 2007]. The larger, semidiurnal tide dominates flow in Southampton Water, however, and little is documented about changes in circulation during the 'young flood stand'.

5.2. Processes Controlling Sediment Resuspension

[44] In the upper Swan River estuary, the timing of maximum vertical shear coincides with the intratidal oscillation which occurs on the flood tide several hours after low water (Figure 9c). Could this oscillation, which is really just a small pause in the barotropic pressure gradient, have produced sufficient vertical shear to mix and destratify strong vertical salinity gradients? Moreover, what mechanisms control the recurring turbidity events in the upper estuary that are associated with intratidal oscillations?

[45] Sharp changes in water level gradients in the Ems-Dollard estuary were directly associated with a turbulent exchange of sediments [*van der Ham et al.*, 2001], but corresponding near-bed stresses from mean currents were high at these times. For the Swan River, the rate of change in water level did vary several times during the flood tide. But since mean currents were less than 0.1 ms^{-1} bed stresses were always below threshold criteria for mobilization, at least when estimated from the standard quadratic stress law and the use of the Shields diagram. High Reynolds stresses in the absence of fast near-bed currents can indicate the possibility of internal waves interacting with the bottom boundary layer as noted by *Dyer et al.* [2004]. However, the combination of high Reynolds stresses and negative Reynolds fluxes are more likely to be the downward flux of material via instabilities at the pycnocline. When the density layer thickness (h) is approximately the same as the shear layer thickness (δ), i.e., $R = h/\delta \approx 1$ then instabilities can take the form of Kelvin-Helmholtz (K-H) instabilities [*Tedford et al.*, 2009]. Immediately prior to the breakdown of stratification (Figure 9c) R was 0.8, slightly less than 1, which suggests K-H instabilities that exhibit large overturns in density were responsible for the observed downward transport of in situ material (suspended sediment, organic matter, suspended biota).

[46] Between 13:30 to 14:30 h on day 353, strong vertical gradients in both salinity and flow are rapidly eroded (Figures 9c and 9d). We propose that differential transport of salt due to the small change in barotropic pressure during the intratidal oscillation is the catalyst for these substantial differences in U(z) and $\rho(z)$ over one hour. Anomalous responses from a low-energy stratified lake (Lake Alpanach), found that near-bed current profiles differed markedly from those obtained from the 'law-of-the-wall' theory within 0.5 m of the bed. A phase lag (of ~1.5 h) between current velocity and turbulence kinetic energy was evident with behavior strongly influenced by an oscillating bottom boundary induced by a seiche [*Lorke et al.*, 2002]. Furthermore, the observed velocity profiles from Lake Alpnach, for the bottom boundary layer resembled those obtained

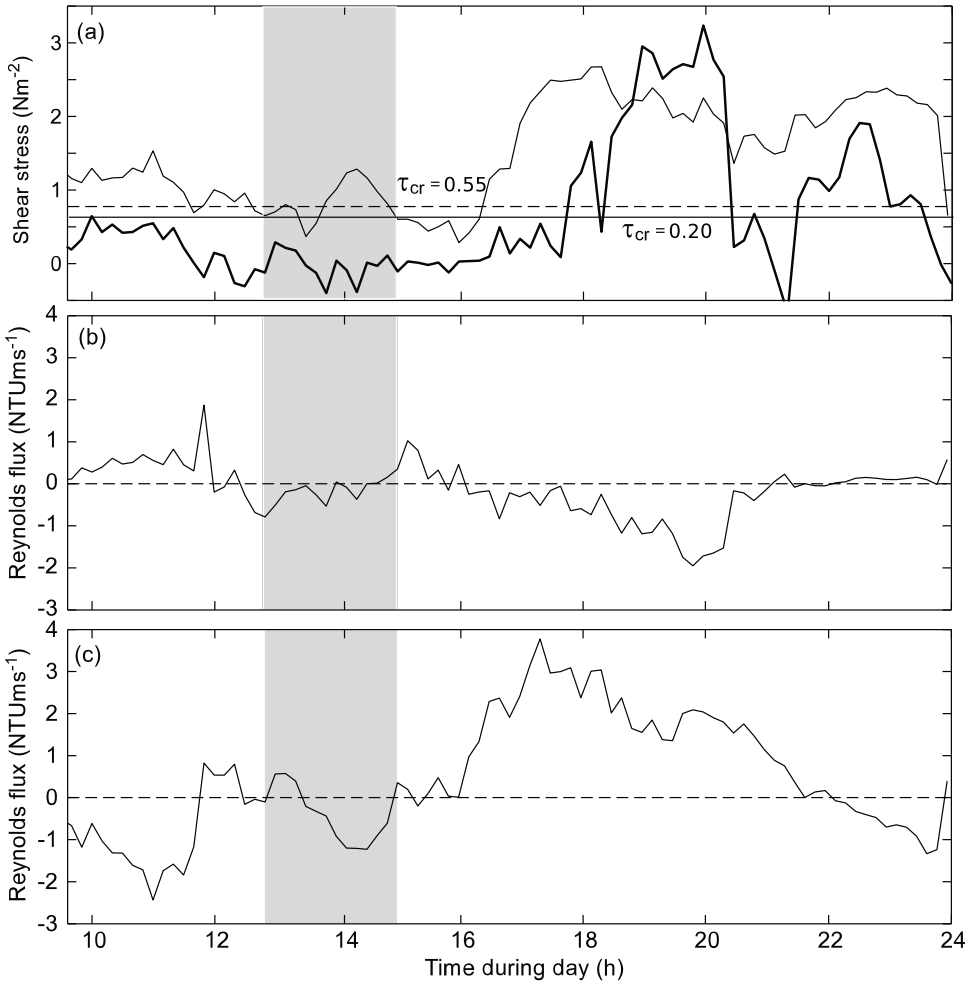

Figure 15. The flood tide on day 353 in 2002. (a) TKE shear stress (thin line) and Reynolds stress (thick line). The dashed, horizontal line is the critical threshold, τ_{cr}, for combined mud/sand sediments (0.55 Nm^{-2}) in the Swan River estuary and the solid, horizontal line is the threshold for active turbulence from *Dyer et al.* [2004]. (b) Turbulent fluxes of turbidity in the horizontal, u′c′, direction, and (c) turbulent fluxes of turbidity in the vertical, w′c′, direction. The dashed, horizontal line in Figures 15b and 15c is the zero crossing for horizontal and vertical fluxes. In Figure 15b positive is upstream and negative the downstream fluxes, and in Figure 15c positive is away from the bed and negative towards the bed.

from Stokes' oscillatory boundary layer theory [*Stokes*, 1851]. Differential horizontal transport in the bottom boundary layer of water of different densities produced unstable vertical stratification and hence additional turbulent kinetic energy for vertical mixing [*Lorke et al.*, 2002].

[47] Vertical profiles obtained for the Swan River (Figures 9a–9h) show a distinct velocity maximum about 1 m from the bed as described by Stokes second problem [*Stokes*, 1851]. These profiles evolve temporally and when coupled with vertical density gradients water column stability is strained. An attempt to capture the Stokes' flow was made numerically, but without being able to assign a forcing frequency (from *Lorke et al.* [2002] a seiche induced oscillation was used) and an adequate turbulence closure model to validate the presence of an oscillating boundary layer, we could not examine this finding further. It was highly encouraging that *Etemad-Shahidi and Imberger* [2002] found increased dissipation by about one order of magnitude at mid-depth in the lower Swan River estuary, but could not attribute this to either instrument errors or a physical mechanism (i.e., internal waves).

[48] Large near-bed Reynolds stresses also exceeded the erosion threshold near to the end of the flood tide. Active turbulence in the vertical direction causes an upward flux of sediment for almost six hours. With relatively weakened salinity stratification, at this time, sediment could be mobilized and transported higher into the water column than it could have been earlier in the flood tide. Bed sediments available for entrainment and resuspension were sandy muds with high organic content. The stickiness of these types of sediments could increase the critical threshold of erosion from 0.55 up to ~2.5 Nm^{-2}, estimated for the Cardiff estuary [*Whitehouse et al.*, 2000], which has a similar mud:sand ratio and organic content as upper Swan River estuary sediments. Accordingly, the duration of events could be reduced to only 1 to 2 hours late in the flood tide at either

18 or 20 h depending on the method used to determine shear stresses.

[49] Intratidal oscillations modified the vertical current structure of flow that were the physical drivers of turbulent instabilities, substantial destratification, and sediment resuspension during the flood tide. Our findings would be applicable to other estuaries that experience intratidal oscillations. For example, the 'young flood stand' in Southampton Water seems a likely candidate whereby advection and stratification would compete at intratidal timescales. Since the generation of tidal inequalities in semidiurnal systems is by bed friction, if such oscillations are observed, they are expected to be persistent mechanisms in an estuary.

6. Conclusions

[50] 1. Diurnal tidal systems differ markedly from the well-observed semidiurnal estuaries. While tidal range varies over the fortnightly cycle, as per tidal conventions, the frequency of the tide can change due to varying inputs from the lunar and solar cycles. For example, close to the vernal equinox, tidal oscillations have a diurnal frequency when tidal range was maximal (or a tropic tide) but tidal frequency was twice per day in the subsequent minimum tidal range just 3 to 4 days later. Near to the Austral solstice, however, both maximum and minimum tidal ranges had a once per day frequency that is expected from tidal theory.

[51] 2. At the tidal timescale the presence of an intratidal oscillation is a recurring feature during the flood tide. Near to the Austral summer solstice, intratidal oscillations of 0.1 m were maximal and lasted for 2 to 3 hours. Current velocities were static and weak during the intratidal oscillation and increased again to almost vertically uniform, up estuary velocities of 0.1 ms^{-1}. Despite such low near-bed current velocities, not sufficiently large enough to initiate sediment mobilization, large turbidity events up to 250 NTUs occur during the intratidal oscillations.

[52] 3. The variable rate of change in water level several hours after low water, starting at 12:30 h and concluding at ~14:30, caused current reversal and substantial vertical shear at the end of this period. Within a 1-hour time frame, turbulent instabilities generated by vertical shear resulted in destratification of the water column; top-to-bottom differences in salinity (ΔS) decreased from 3.5 to less than 0.3 by the end of the intratidal oscillation. The highest estimate of ε was $\sim 9 \times 10^{-4}$ $m^2 s^{-3}$, but most ϵ estimates were at least an order of magnitude smaller.

[53] 4. Reynolds stresses of ~1 Nm^{-2} exceeded critical threshold values of 0.55 Nm^{-2} and together with negative Reynolds fluxes (in the vertical) indicate a net downward transport of material. These turbulent instabilities induced by the breakdown of stratification at the pycnocline were responsible for vertical transport of in situ material towards the bed and were responsible for high turbidity events during the intratidal oscillations.

[54] **Acknowledgments.** This study was undertaken with funding obtained from an Australian Research Council Strategic Partnerships with Industry, Research and Training (ARC SPIRT) grant (C00002550) in collaboration with the Water and Rivers Commission, Department of Environment. The authors thank the Swan River Trust for their help in collecting the field data. This work was carried out while J.M. O'Callaghan was in receipt of an Australian Postgraduate Award (Industry) from the University of Western Australia. This is contribution SESE 068 from the School of Environmental Systems Engineering, University of Western Australia. The suggestions of two anonymous reviewers greatly improved this manuscript.

References

Aubrey, D. G., and P. E. Speer (1985), A study of non-linear tidal propagation in shallow inlet estuarine systems Part I: Observations, *Estuarine Coastal Shelf Sci.*, *21*, 185–205.

Becker, M. L., R. A. Luettich Jr., and H. Seim (2009), Effects of intratidal and tidal range variability on circulation and salinity structure in the Cape Fear River Estuary, North Carolina, *J. Geophys. Res.*, *114*, C04006, doi:10.1029/2008JC004972.

Blanton, J. O., H. Seim, C. Alexander, J. Amft, and G. Kineke (2003), Transport of salt and suspended sediments in a curving channel of a coastal plain estuary: Satilla River, GA, *Estuarine Coastal Shelf Sci.*, *57*, 993–1006, doi:10.1016/S0272-2.

Cooper, S. R., and G. S. Brush (1993), A 2,500-year history of anoxia and eutrophication in Chesapeake Bay, *Estuaries*, *16*(3B), 617–626.

Deines, K. L. (1999), Backscatter estimation using broadband acoustic Doppler current profilers, paper presented at Sixth Working Conference on Current Measurements, Inst. of Electr. and Electr. Eng., San Diego, Calif., 11–13 Mar.

Dyer, K. R. (1997), *Estuaries: A Physical Introduction*, 2nd ed., 195 pp., John Wiley, New York.

Dyer, K. R., M. C. Christie, and A. J. Manning (2004), The effects of suspended sediment on turbulence within an estuarine turbidity maximum, *Estuarine Coastal Shelf Sci.*, *59*, 237–248.

Etemad-Shahidi, A., and J. Imberger (2002), Anatomy of turbulence in a narrow and weakly stratified estuary, *Mar. Freshwater Res.*,*53*, 757–768.

Hamilton, D. P., T. U. Chan, B. J. Robson, and B. R. Hodges (2000), The effects of freshwater flows and salinity on phytoplankton biomass and composition in an urban estuary, the Swan River, Western Australia, paper presented at 3rd International Hydrology and Water Resources Symposium, Perth, Inst. of Eng. (Aust.), West. Aust., Australia, 20–23 Nov.

Hamilton, D. P., T. Chan, M. S. Robb, C. B. Pattiaratchi, and M. Herzfeld (2001), The hydrology of the upper Swan River Estuary with focus on an artificial destratification trial, *Hydrol. Processes*,*15*(13), 2465–2480.

Hodgkin, E. P., and V. Di Lollo (1958), The tides of south-western Australia, *J. R. Soc. West. Aust. 41*, 42–54.

Hoitink, A. J. F., and P. Hoekstra (2005), Observations of suspended sediment from ADCP and OBS measurements in a mud-dominated environment, *Coastal Eng.*, *52*, 103–118.

Hoitink, A. J. F., P. Hoekstra, and D. S. van Maren (2003), Flow asymmetry associated with astronomical tides: Implications for the residual transport of sediment, *J. Geophys. Res.*, *108*(C10), 3315, doi:10.1029/2002JC001539.

Imberger, J., and G. Ivey (1991), On the nature of turbulence in a stratified fluid. Part 2: Application to lakes, *J. Phys. Oceanogr.*, *21*, 659–680.

Kim, Y. H., and G. Voulgaris (2008), Lateral circulation and suspended sediment transport in a curved estuarine channel: Winyah Bay, SC, USA, *J. Geophys. Res.*, *113*, C09006, doi:10.1029/2007JC004509.

Lemckert, C. J., J. P. Antenucci, A. Saggio, and J. Imberger (2004), Physical properties of turbulent benthic boundary layers generated by internal waves, *J. Hydrol. Eng.*, *130*(1), 58–69.

Levasseur, A., L. Shi, N. C. Wells, D. A. Purdie, and B. A. Kelly-Gerreyn (2007), dimensional hydrodynamic model of estuarine circulation with an application to Southampton Water, UK, *Estuarine Coastal Shelf Sci.*, *73*, 753–767.

Lorke, A., L. Umlauf, T. Jonas, and A. Wuest (2002), Dynamics of turbulence in low-speed oscillating bottom boundary layers of stratified basins, *Environ. Fluid Mech.*, *2*, 291–313.

Mitchener, H., and H. Torfs (1996), Erosion of mud/sand mixtures, *Coastal Eng.*, *29*, 1–25.

Nepf, H. M., and W. R. Geyer (1996), Intratidal variations in stratification and mixing in the Hudson estuary, *J. Geophys. Res.*, *101*(C5), 12,079–12,086, doi:10.1029/96JC00630.

O'Callaghan, J. M. (2005), Tidal and sediment dynamics of a partially mixed, micro-tidal estuary, Ph.D. thesis, Dep. of Environ. Eng., Univ. of West. Aust., Perth, West. Aust., Australia.

O'Callaghan, J. M., C. B. Pattiaratchi, and D. P. Hamilton (2007), The response of circulation and salinity in a micro-tidal estuary to sub-tidal oscillations in coastal sea surface elevation, *Cont. Shelf Res.*, *27*, 1947–1965.

Peters, H. (1997), Observations of stratified turbulent mixing in an estuary: Neap to Spring variations during high river flow, *Estuarine Coastal Shelf Sci.*, *45*, 69–88.

Peters, N. E., and R. Donohue (2001), Nutrient transport in the Swan-Canning estuary, Western Australia, *Hydrol. Processes*, *15*(13), 2555–2578.

Pugh, D. T. (1987), *Tides, Surges and Mean Sea-Level*, 472 pp., John Wiley, New York.

Pugh, D. T. (2004), *Changing Sea Levels*, 265 pp., Cambridge Univ. Press, Cambridge, U. K.

Ranasinghe, R., and C. Pattiaratchi (2000), Tidal inlet velocity asymmetry in diurnal regimes, *Cont. Shelf Res.*, *20*, 2347–2366.

Ridd, P. V., and P. Larcombe (1994), Biofouling control for optical back-scatter suspended sediment sensors, *Mar. Geol.*, *46*, 255–258.

Simpson, J. H., J. Brown, J. Matthews, and G. Allen (1990), Tidal straining, density currents, and stirring in the control of estuarine stratification, *Estuaries*, *13*(2), 125–132.

Spencer, R. S. (1956), Studies in Australian estuarine hydrology. Part II. The Swan River, *Aust. J. Mar. Freshwater Res.*, *7*, 196–253.

Stacey, M. T., J. R. Burau, and S. G. Monismith (2001), Creation of residual flows in a partially stratified estuary, *J. Geophys. Res.*, *106*(C8), 17,013–17,037.

Stevens, C. L., and M. J. Smith (2004), Temperature microstructure beneath surface gravity waves, *J. Atmos. Oceanic Tech.*, *21*, 1747–1757.

Stokes, G. G. (1851), On the effect of the internal friction of fluids on the motion of pendulums, *Trans. Cambridge Philos. Soc.*, *9*, 8–106.

Tedford, E. W., J. R. Carpenter, R. Pawlowicz, R. Pieters, and G. A. Lawrence (2009), Observation and analysis of shear instability in the Fraser River estuary, *J. Geophys. Res.*, *114*, C11006, doi:10.1029/2009JC005313.

Tennekes, H., and J. L. Lumley (1994), *A First Course in Turbulence*, 2nd ed., MIT Press, Cambridge, U. K.

Uncles, R. J. (2002), Estuarine physical processes research: Some recent studies and progress, *Estuarine Coastal Shelf. Sci.*, *55*, 829–856.

van de Kreeke, J., C. M. Day, and H. P. J. Mulder (1997), Tidal variations in suspended sediment concentration in the Ems estuary: Origin and resulting sediment flux, *J. Sea Res.*, *38*, 1–16.

van der Ham, R., H. L. Fontijn, C. Kranenburg, and J. C. Winterwerp (2001), Turbulent exchange of fine sediments in a tidal channel in the Ems/Dollard estuary. Part I: Turbulence measurements, *Cont. Shelf Res.*, *21*, 1605–1628.

van Maren, D. S., P. Hoekstra, and A. J. F. Hoitlink (2004), Tidal flow asymmetry in the diurnal regime: Bed-load transport and morphologic changes around the Red River Delta, *Ocean Dyn.*, *54*, 424–434, doi:10.1007/s10236-0085-0.

van Rijn, L. C. (1989), Handbook-sediment transport by currents and waves, *Report H 461*, Delft Hydraul., Delft, Netherlands.

Weisberg, R. H., and L. Zheng (2003), How estuaries work: A Charlotte Harbor example, *J. Mar. Res.*, *61*, 635–657 doi:10.1357/002224003771815981.

Whitehouse, R., R. Soulsby, W. Roberts, and H. Mitchener (2000), *Dynamics of Estuarine Muds: A Manual for Practical Application*, 210 pp., Thomas Telford, London.

Woodworth, P. L., D. L. Blackman, D. T. Pugh, and J. M. Vassie (2005), On the role of diurnal tides in contributing to asymmetries in tidal probability distribution functions in areas of predominantly semi-diurnal tide, *Estuarine Coastal Shelf Sci.*, *64*, 235–240.

Wright, L. D., L. C. Schaffner, J. P.-Y. Maam (1997), Biological mediation of bottom boundary layer processes and sediment suspension in the lower Chesapeake Bay, *Mar. Geol.*, *141*, 27–50.

D. P. Hamilton, Department of Biological Sciences, University of Waikato, Private Bag 3105, 3240 Hamilton, New Zealand.

J. M. O'Callaghan, National Institute of Water and Atmosphere, Private Bag 14-901, 6021 Wellington, New Zealand. (j.ocallaghan@niwa.co.nz)

C. B. Pattiaratchi, School of Environmental Systems Engineering, University of Western Australia, 35 Stirling Hwy., Crawley, WA 6009, Australia.